IEICE TRANS. ELECTRON., VOL.E107–C, NO.10 OCTOBER 2024

INVITED PAPER *Special Section on Analog Circuits and Their Application Technologies*

Advancements in Terahertz Communication: Harnessing the 300 GHz Band for High-Efficiency, High-Capacity Wireless Networks

Minoru FUJISHIMA[†a)], ***Fellow***

SUMMARY In this paper, we delve into wireless communications in the 300 GHz band, focusing in particular on the continuous bandwidth of 44 GHz from 252 GHz to 296 GHz, positioning it as a pivotal element in the trajectory toward 6G communications. While terahertz communications have traditionally been praised for the high speeds they can achieve using their wide bandwidth, focusing the beam has also shown the potential to achieve high energy efficiency and support numerous simultaneous connectivity. To this end, new performance metrics, EIRP_{λ} and EINF_{λ}, are introduced as important benchmarks for transmitter and receiver performance, and their consistency is discussed. We then show that, assuming conventional bandwidth and communication capacity, the communication distance is independent of carrier frequency. Located between radio waves and light in the electromagnetic spectrum, terahertz waves promise to usher in a new era of wireless communications characterized not only by high-speed communication, but also by convenience and efficiency. Improvements in antenna gain, beam focusing, and precise beam steering are essential to its realization. As these technologies advance, the paradigm of wireless communications is expected to be transformed. The synergistic effects of antenna gain enhancement, beam focusing, and steering will not only push high-speed communications to unprecedented levels, but also lay the foundation for a wireless communications landscape defined by unparalleled convenience and efficiency. This paper will discuss a future in which terahertz communications will reshape the contours of wireless communications as the realization of such technological breakthroughs draws near.

key words: *terahertz communication, wireless networks, 300 GHz band, beamforming, phased array, high-efficiency communication, high-capacity communication, antenna gain, wireless beam control, terahertz transceiver*

1. Introduction

In recent years, the field of wireless communication has witnessed remarkable advancements in data rates [1]. Anticipating the onset of the sixth generation (6G) around 2030, data rates exceeding 100 Gb/s are expected to become a reality [2]. A pivotal technology driving this progress is sub-terahertz communication, positioned as a key development for 6G. Beyond its role in achieving ultrahigh-speed communication, sub-terahertz communication harbors the potential to enable high-efficiency communication and numerous simultaneous connectivity. This paper aims to discuss the substantial capabilities of sub-terahertz communication beyond just achieving high-speed communication.

To realize sub-terahertz communication, two major technological approaches come into play: the photonics approach [3]–[6] and the electronics approach [7]–[29]. Generating terahertz waves using optical mixing from signals in the optical fibers of the backbone network proves advantageous for incorporating sub-terahertz communication as part of the backbone network. However, realizing a fully photonic transceiver faces challenges, requiring electronics circuits for amplifying weak received signals. Additionally, the photonics approach, relying on servers in the backbone network (typically high power-consuming), is not inherently suited for low-power consumption. On the contrary, the electronics approach, leveraging easily miniaturized and low-power consuming components, is suitable not only for the backbone network but also for terminal applications, albeit requiring EO/OE conversion to connect with the optical fiber network.

Our research has focused on the electronics approach, utilizing readily producible CMOS integrated circuits, in the development of sub-terahertz transceivers [18]–[29]. This paper provides an overview of sub-terahertz transceivers employing CMOS integrated circuits and engages in a discussion about the future of sub-terahertz. Exploring how wireless communication data rates are determined, evaluating transceiver performance, and unveiling the key role of beamforming in enhancing data rates will be pivotal aspects of this discussion. Furthermore, we introduce sub-terahertz CMOS receivers capable of two-dimensional manipulation through the use of beamforming, offering enhanced capabilities in the sub-terahertz spectrum.

2. 300 GHz CMOS Transceiver

The ever-increasing demand for higher data rates in wireless communication has led to a significant rise in carrier frequencies. As depicted in Fig. 1, recent developments extend carrier frequencies beyond millimeter waves into the terahertz range. Notably, the 300 GHz band has emerged as a focal point of attention. Traditionally allocated for wireless communication, particularly in mobile and land-fixed communication, the 300 GHz band witnessed an expansion during the 2019 World Radiocommunication Conference [26]. This expansion, from 252 GHz to 296 GHz, opened up a broad frequency spectrum of 44 GHz for wireless communication. The utilization of the sub-terahertz 300 GHz band holds the promise of achieving data rates exceeding 100 Gb/s in wireless communication.

Manuscript received December 4, 2023.
Manuscript publicized March 8, 2024.

[†]Hiroshima University, Higashi-hiroshima-shi, 739–8530 Japan.
a) E-mail: fuji@hiroshima-u.ac.jp

DOI: 10.1587/transele.2023CTI0002

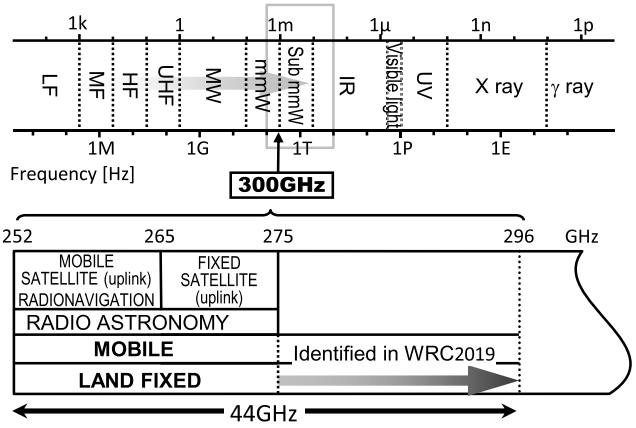

Fig. 1 The carrier frequency for wireless communications has been increasing year by year to reach terahertz frequencies in order to increase the data rate. Among these, the 300 GHz band is expected to realize ultrahigh-speed wireless communications because it can use a continuous frequency band of 44 GHz [30].

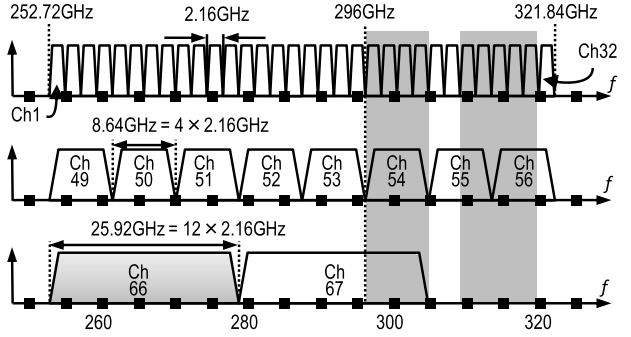

Fig. 2 In IEEE 802.15.3d, channel allocation in the 300 GHz band is proposed. Among these, we focused on channel 66, which has a frequency bandwidth of 25.92 GHz [25], [26], [31].

2.1 300 GHz Single-Chip CMOS Transceiver [25], [26]

2.1.1 Channel Selection

In accordance with IEEE Standard 802.15.3d, a channel allocation proposal covering the 252 GHz to 322 GHz range as depicted in Fig. 2, with relatively low atmospheric attenuation, includes the 300 GHz band [31]. Among several channels, our focus lies on Channel 66, spanning a frequency bandwidth of 25.92 GHz. Notably, this bandwidth is 12 times larger than the 2.16 GHz frequency bandwidth of a single channel in the 60 GHz band.

2.1.2 Challenges and Solutions in Sub-Terahertz CMOS Transceiver

The maximum operating frequency (fmax) of NMOSFET in CMOS integrated circuits is approximately 300 GHz. Consequently, conventional transceiver components such as power amplifiers (PAs), low-noise amplifiers (LNAs), and local oscillators (LOs) cannot be employed as depicted in Fig. 3, necessitating the construction of a transceiver without these essential components.

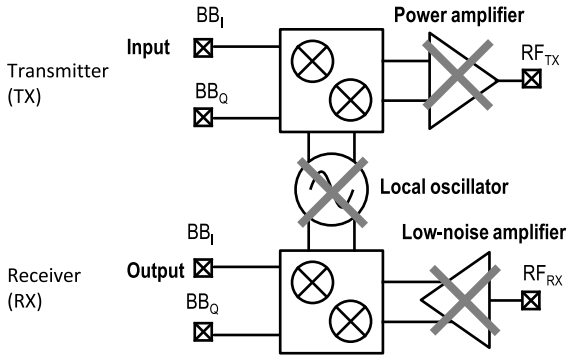

Fig. 3 The maximum operating frequency (fmax) of transistors used in CMOS integrated circuits is about 300 GHz. Therefore, power amplifiers, low-noise amplifiers, and fundamental local oscillators normally used in wireless transceivers cannot be used [32], [33].

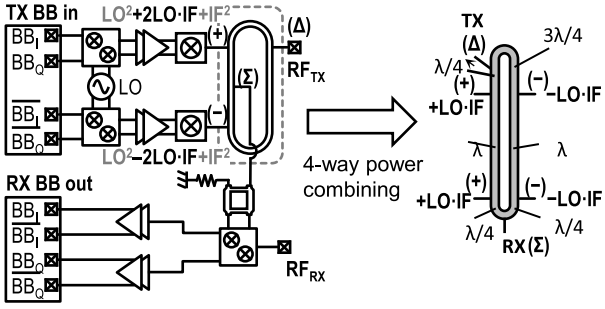

Fig. 4 Architecture of our realized 300 GHz single-chip transceiver. To integrate the transmitter and receiver, we used the in-phase and differential outputs of a rat race circuit [25], [26].

The architecture of the proposed 300 GHz transceiver, as illustrated in Fig. 4, addresses these challenges. In the transmission mode, a rat-race circuit is connected to the output, utilizing its in-phase (Σ) and differential (Δ) output ports. During transmission, the baseband input (TX_{BBin}) signal undergoes up-conversion to intermediate frequency (IF) through the first mixer. This mixer not only produces the IF signal but also leaks the LO signal to the output. Therefore, the LO and IF signals are combined and amplified to go into a second mixer, called a square mixer. This mixer outputs the squared signal of the input, with the desired RF signal at 2LO · IF in the 300-GHz band. However, the unwanted components LO^2 and IF^2 are also output simultaneously. To eliminate unwanted components, a second path is incorporated, generating an LO – IF signal. By employing a rat-race circuit, the undesired LO^2 and IF^2 components are subtracted, leaving only the amplified desired signal.

In receiver mode, the TX_{BBin} signals are terminated, allowing both paths of the first mixer to leak only the LO signal. This LO signal is fed into the square mixer, generating LO^2. This LO^2 is fed to the rat-race circuit and amplified by power combining by using its in-phase port (Σ). This amplified LO^2 is fed into a 90-degree hybrid circuit, producing the I/Q LO signals for down-converting the 300 GHz RF

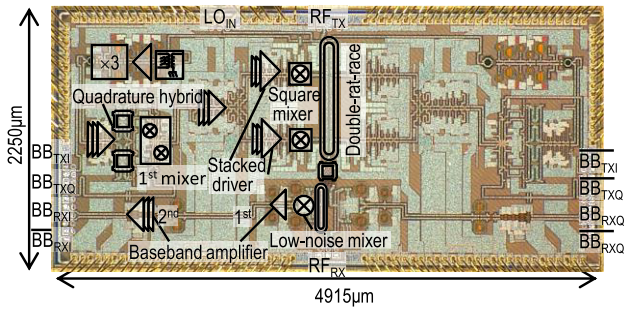

Fig. 5 Chip photomicrograph of a 300-GHz CMOS single-chip transceiver, in which the outputs of four square mixers are then power-combined to enhance the output of a 300-GHz signal [25], [26].

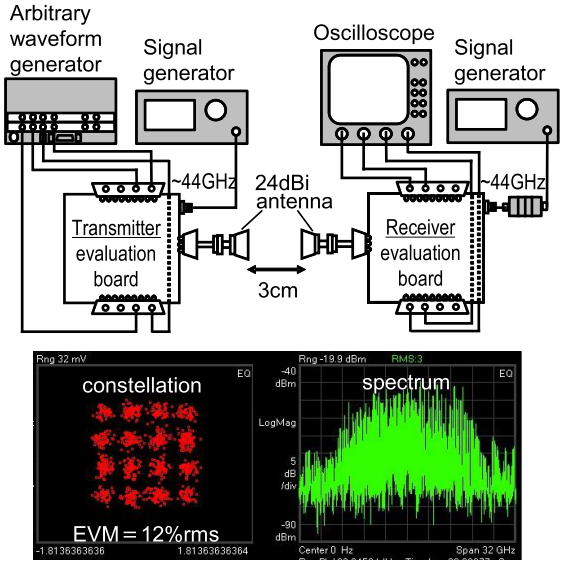

Fig. 6 Experiments on a 300-GHz CMOS single-chip transceiver. A transmitter and receiver evaluation boards are created and 300 GHz signals are extracted using waveguide probes. Data rates of up to 80 Gb/s are achieved [25], [26].

signal directly to the baseband.

Figure 5 presents a photomicrograph of the prototype single-chip CMOS transceiver, fabricated using a 40 nm bulk CMOS process. To enhance the output power of the square mixer, a circuit called a double rat race with four inputs is used for power combining.

2.1.3 Experimental Overview of 300 GHz Single-Chip Transceiver

Figure 6 outlines the experimental setup for the 300 GHz single-chip transceiver. Evaluation boards for both transmitter and receiver are created using the same chip. The 300 GHz RF signal is extracted using a waveguide probe, connected to a WR3.4 horn antenna. The frequency aligns with IEEE 802.15.3d Channel 66. Employing a 16QAM signal, the transceiver achieved a maximum data rate of 80 Gb/s in a single channel. Notably, despite the absence of a power amplifier, utilizing power combining, the output saturation

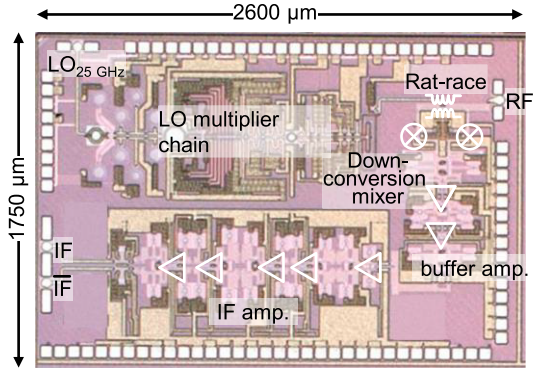

Fig. 7 Chip photomicrograph of a 300-GHz CMOS receiver for use in mounting tests, created using a 40-nm CMOS process [27], [28].

power of the transmitter reached −1.6 dBm.

In conclusion, the presented 300 GHz CMOS transceiver demonstrates an architecture overcoming the challenges posed by the sub-terahertz frequency band. The experimental results showcase promising performance in achieving high data rates in wireless communication, opening avenues for future research and development in this domain.

2.2 Packaging Technology for 300 GHz CMOS Receiver [27], [28]

2.2.1 Receiver CMOS Chip and Packaging Overview

In the pursuit of pushing the boundaries of wireless communication into the sub-terahertz frequency range, we have developed packaging technology for a 300 GHz CMOS receiver. Figure 7 presents a photomicrograph of the CMOS chip utilized in the packaging process, fabricated using a 40 nm bulk CMOS process. The CMOS receiver adopts a low-noise amplifier-less (LNA-less) architecture. The receiver generates a 225 GHz LO signal through ninefold up-conversion of the externally supplied 25 GHz signal, which is then supplied to the down-conversion mixer. The down-conversion mixer transforms the 265 GHz RF signal into a 40 GHz IF signal.

The CMOS chip is implemented using a flip-chip mounting on a printed circuit board (PCB) made of organic dielectric material, as illustrated in Fig. 8. The PCB boasts eight layers of wiring and is equipped with a WR3.4 waveguide flange on the opposite side of the chip implementation. The PCB facilitates not only power supply and conventional high-frequency wiring but also the transition of the 300 GHz band signal from a waveguide to a transmission line.

Figure 9 provides detailed insights into the transmission line to waveguide conversion implemented on the PCB. The CMOS substrate is flip-chip mounted on the first layer (L1) and connected to the PCB through coplanar waveguides (CPW) and 50-μm diameter GSG (ground-signal-ground) stud bumps with a 75-μm pitch. The PCB incorporates a pseudo-waveguide structure achieved by stacking rectangu-

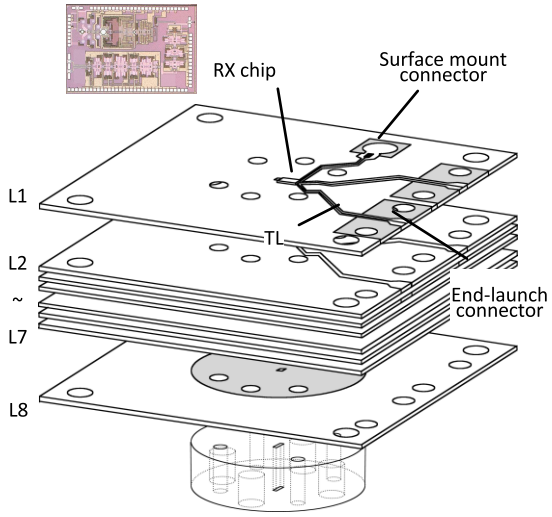

Fig. 8 Overall view of a 300-GHz CMOS receiver being mounted on a board; the CMOS chip is flip-chip mounted on the board and the WR3.4 waveguide flange is attached on the opposite side [27], [28].

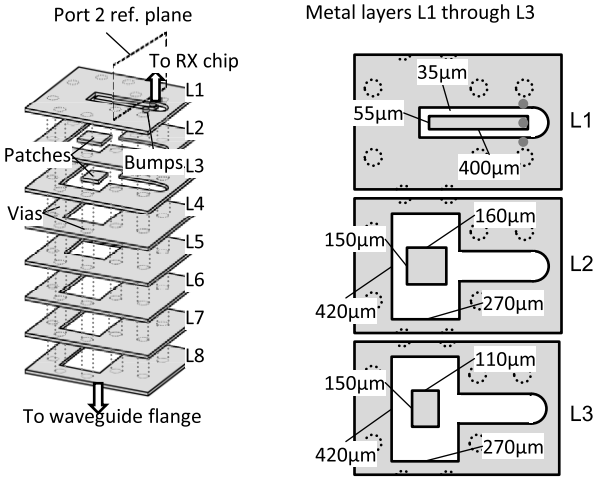

Fig. 9 Structure of the board on which the 300-GHz band CMOS receiver is mounted. 8-layer printed circuit board is used, with the CMOS chip on the first layer (L1) and the WR3.4 waveguide flange on the eighth layer (L8) [27], [28].

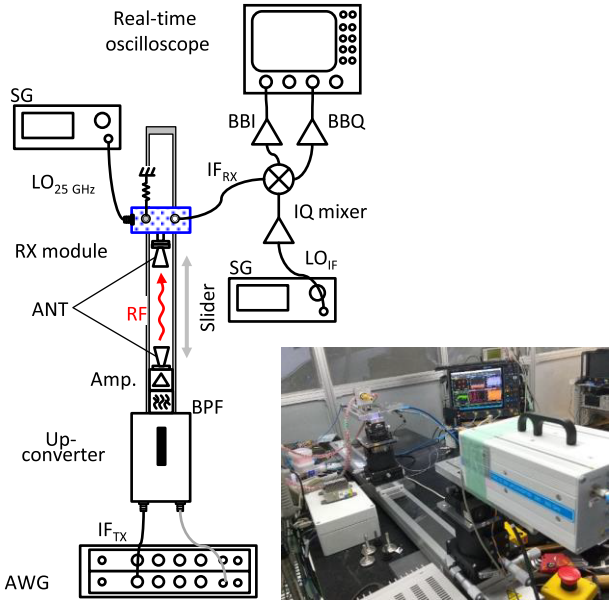

Fig. 10 Over-the-air measurement of a 300 GHz CMOS receiver module. The transmitter is a commercial frequency up-converter with a power amplifier [27], [28].

Constellation	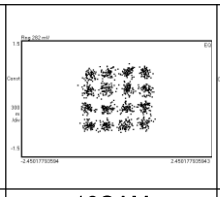	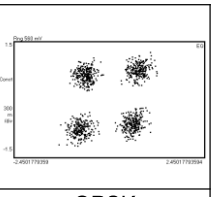
Modulation	16QAM	QPSK
Distance [cm]	6	100
EVM [%rms]	13.04	25.93
BER	2.27×10^{-4}	5.75×10^{-5}
Center frequency [GHz]	265.68	266.76
Symbol rate [Gbaud]	19	2.16
Data rate [Gbit/s]	76	4.32

Fig. 11 Over-the-air measurement results. Maximum 76 Gb/s was achieved at a communication distance of 6 cm, and 4.32 Gb/s at a communication distance of 1 m [27], [28].

lar cutouts in the metal layers. Two different-sized patches are employed to couple with this pseudo-waveguide. The stacking of these two patches realizes dual resonance, enhancing the bandwidth. The upper-layer patch is electrically coupled to the open end of the CPW.

2.2.2 Over-the-Air Measurements and Results

The module's over-the-air performance was evaluated using the measurement setup depicted in Fig. 10. An arbitrary waveform generator (AWG) generated the modulated IF signal, generating a 300 GHz signal through a commercial block up-converter. The generated signal was amplified by a power amplifier and radiated through a horn antenna. The CMOS receiver module, connected to the horn antenna, down-converted the received signal to the IF signal. The IF signal is down-converted to baseband by a quadrature mixer and demodulated and analyzed by a real-time oscilloscope. Figure 11 presents the measurement results, showcasing a maximum data rate of 76 Gbit/s with 16QAM signals at a communication distance of 6 cm. Additionally, at a communication distance of 1 m, a maximum data rate of 4.32 Gbit/s was achieved using QPSK signals.

In conclusion, the presented 300 GHz CMOS receiver module demonstrates overcoming the packaging challenges posed by the sub-terahertz frequency band. Experimental results show promising performance to achieve high data rates over-the-air.

3. Wireless Communication and Communication Range in the Context of Terahertz Technology

This section delves into the evolving landscape of wireless communication, particularly in the terahertz frequency range, focusing on achieving high data rates. As we explore advancements, there is an emerging need to broaden coverage for Beyond 5G networks. Traditionally, it has been noted that coverage decreases as carrier frequency is increased. This raises the question: why does coverage tend to decrease with higher carrier frequencies? Ideally, the quest is to reconcile ultrahigh-speed data rates with extreme coverage. This section aims to theoretically analyze pathways for the evolution of wireless communication towards this ideal.

3.1 Theoretical Analysis

Applying Shannon-Hartley theorem, communication capacity C is given by

$$C = B\log_2\left(1+\frac{S}{N}\right), \tag{1}$$

where B is the bandwidth, and S and N are the signal and noise power, respectively. When adapted for wireless communication,

$$C = B\log_2\left(1+\frac{P_\mathrm{r}}{kTB\cdot\mathrm{NF}}\right), \tag{2}$$

where P_r is the received power, k is Boltzmann's constant, T is absolute temperature, and NF is the noise figure of the receiver [32], [33]. The relationship between communication capacity C and bandwidth B for received powers of 0.1 μW, 1 μW, and 10 μW is illustrated in Fig. 12. The graph highlights the trade-off between bandwidth limitations and power constraints. To increase communication capacity, it is evident that widening the bandwidth alone is insufficient; an increase in received power is also necessary.

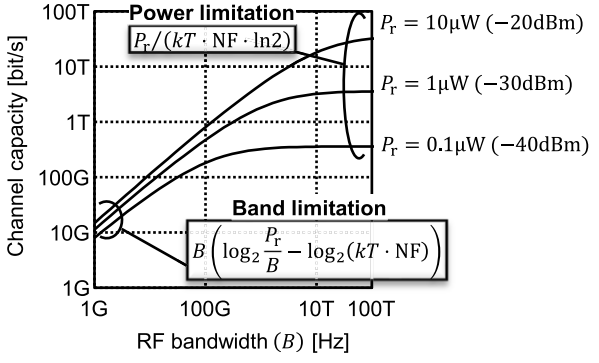

Fig. 12 Relation between communication capacity (C) and RF bandwidth (B) when applying the Shannon-Hartley theorem to wireless communications. Three different received power (P_r) were calculated for 0.1 μW, 1 μW, and 10 μW. Here, T = 290 K, NF = 20 dB [32], [33].

3.2 Communication Range Analysis

The received power P_r can be expressed through Friis' transmission formula [34] as

$$\frac{P_\mathrm{r}}{P_\mathrm{t}} = G_\mathrm{t}G_\mathrm{r}\left(\frac{\lambda}{4\pi d}\right)^2, \tag{3}$$

where P_t is the transmit power, G_t and G_r are the antenna gains of the transmitter and receiver, respectively, λ is the wavelength, and d is the communication distance. Here by transforming (3), we obtain

$$\frac{P_\mathrm{r}}{P_\mathrm{t}} = \frac{\lambda G_\mathrm{t}}{4\pi}\cdot\frac{\lambda G_\mathrm{r}}{4\pi}\cdot\frac{1}{d^2} = \frac{A_\mathrm{t}}{\lambda}\cdot\frac{A_\mathrm{r}}{\lambda}\cdot\frac{1}{d^2}, \tag{4}$$

where A_t and A_r are the effective antenna areas of the transmitter and receiver, respectively. By defining

$$G_{\lambda\mathrm{t}} \triangleq \frac{\lambda G_\mathrm{t}}{4\pi} = \frac{A_\mathrm{t}}{\lambda} \text{ and} \tag{5}$$

$$G_{\lambda\mathrm{r}} \triangleq \frac{\lambda G_\mathrm{r}}{4\pi} = \frac{A_\mathrm{r}}{\lambda} \tag{6}$$

as the wavelength-normalized antenna gains of the transmitter and receiver as $G_{\lambda\mathrm{t}}$ and $G_{\lambda\mathrm{r}}$, respectively, we obtain

$$\frac{P_\mathrm{r}}{P_\mathrm{t}} = G_{\lambda\mathrm{t}}G_{\lambda\mathrm{r}}\frac{1}{d^2}. \tag{7}$$

This formulation incorporates the wavelength dependency into the wavelength-normalized antenna gains. Consequently, it indicates that if the wavelength-normalized antenna gains do not vary, (7) becomes wavelength-independent. Applying this to (2),

$$d = \sqrt{\frac{G_{\lambda\mathrm{t}}G_{\lambda\mathrm{r}}P_\mathrm{t}}{\left(2^{\frac{C}{B}}-1\right)B\cdot NF\cdot kT}}. \tag{8}$$

When $2^{C/B} \gg 1$, (8) simplifies to obtain

$$d \simeq \sqrt{\frac{G_{\lambda\mathrm{t}}G_{\lambda\mathrm{r}}P_\mathrm{t}}{NF\cdot kT}}\frac{2^{-\frac{C}{2B}}}{\sqrt{B}}. \tag{9}$$

This reveals an inverse relationship between communication distance d and communication capacity C. When bandwidth B is proportional to communication capacity C ($B = \alpha C$), the relationship becomes

$$d \simeq \sqrt{\frac{G_{\lambda\mathrm{t}}G_{\lambda\mathrm{r}}P_\mathrm{t}}{NF\cdot kT}}\frac{2^{-\frac{1}{2\alpha}}}{\sqrt{\alpha}}\frac{1}{\sqrt{C}}. \tag{10}$$

This demonstrates that communication distance inversely scales with the square root of communication capacity. On the other hand, if B is constant:

$$d \simeq \sqrt{\frac{G_{\lambda\mathrm{t}}G_{\lambda\mathrm{r}}P_\mathrm{t}}{NF\cdot kT}}\frac{1}{\sqrt{B}}\left(2^{\frac{1}{2B}}\right)^{-C}. \tag{11}$$

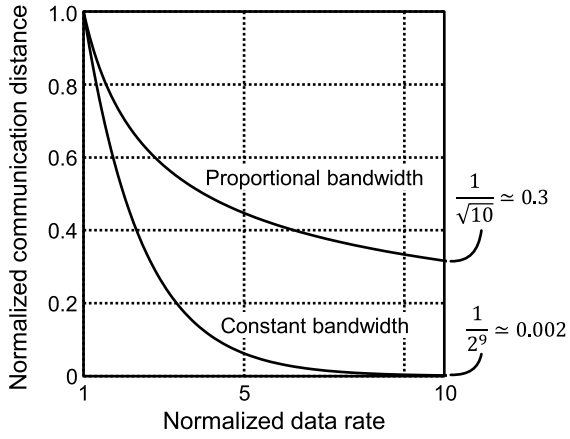

Fig. 13 Comparison of normalized communication distance when bandwidth is increased in proportion to communication capacity (Proportional bandwidth) and when communication capacity is increased with constant bandwidth (Constant bandwidth). In the case of constant bandwidth, the communication distance decreases exponentially.

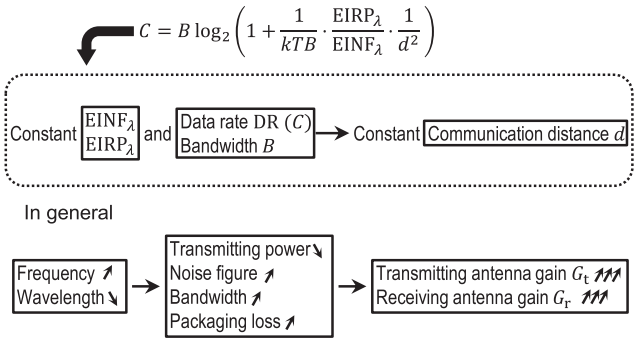

Fig. 14 The relationship between communication capacity, which is determined from wavelength-normalized equivalent isotropic radiated power EIRP_λ and wavelength-normalized equivalent isotropic noise figure EINF_λ, and communication distance. If EIRP_λ, EINF_λ, data rate DR, and bandwidth B are constant, the communication distance remains the same. However, considering the effect of increasing the frequency, it is necessary to increase the antenna gains (G_t, G_r) to obtain the same communication distance.

In this case, communication distance exponentially decreases with increasing communication capacity. A comparison between proportional bandwidth and constant bandwidth scenarios is presented in Fig. 13. The results show that increasing bandwidth significantly outperforms maintaining a constant bandwidth when aiming to increase communication capacity while mitigating a decrease in communication distance. In other words, terahertz communication with room to increase bandwidth is better suited to halt the decrease in communication distance.

3.3 Transceiver Performance Metrics

Here we analyze the performance metrics of the transceiver. From (1), it is the bandwidth B the signal-to-noise ratio S/N of and the receiver that determines the communication capacity. Using (7),

$$\frac{S}{N} = \frac{P_\mathrm{r}}{kTB \cdot \mathrm{NF}} = \frac{1}{kTB} \cdot P_\mathrm{t} G_{\lambda\mathrm{t}} \cdot \frac{G_{\lambda\mathrm{r}}}{\mathrm{NF}} \cdot \frac{1}{d^2} \tag{12}$$

expresses the S/N of the receiver. We now introduce the wavelength-normalized equivalent isotropic radiated power EIRP_λ and the wavelength-normalized equivalent isotropic noise figure EINF_λ as

$$\mathrm{EIRP}_\lambda \triangleq P_\mathrm{t} G_{\lambda\mathrm{t}} = \frac{\lambda}{4\pi} \mathrm{EIRP} \text{ and} \tag{13}$$

$$\mathrm{EINF}_\lambda \triangleq \frac{\mathrm{NF}}{G_{\lambda\mathrm{r}}} = \frac{4\pi}{\lambda} \frac{\mathrm{NF}}{G_\mathrm{r}} \tag{14}$$

as performance metrics for the transmitter and receiver, respectively. Using both, (2) can be set as

$$C = B \log_2 \left(1 + \frac{1}{kTB} \cdot \frac{\mathrm{EIRP}_\lambda}{\mathrm{EINF}_\lambda} \cdot \frac{1}{d^2}\right), \tag{15}$$

which encapsulates the relationship between communication capacity C, bandwidth B, and the transceiver's performance metrics. The conclusion drawn from (15) is summarized in Fig. 14. Assuming EIRP_λ, EINF_λ, C, and B are constant, the communication distance remains constant. This implies that an increase in carrier frequency does not necessarily lead to a decrease in communication distance. However, in reality, increasing the frequency (shortening the wavelength) is often necessary to enlarge both B and C. Additionally, raising the carrier frequency can degrade device performance, resulting in reduced output power, increased noise figure, and significant implementation losses. To maintain communication distance while increasing C, it becomes imperative to enhance EIRP_λ and reduce EINF_λ. In essence, increasing both transmitter and receiver antenna gains is essential. Note that for a given antenna size, antenna gain increases inversely as the square of the wavelength. Increasing the antenna size relative to the wavelength requires the use of lenses and concave mirrors, as well as increasing the size of the phased array that can control the beam direction.

Achieving extremely high data rates over long distances can be exemplified by satellite-to-satellite laser links (ISLL). These links operate over vast distances (6000 km) at a data rate of 10 Gb/s [35]. Although the laser's wavelength is much shorter and frequency much higher than terahertz, the use of highly gainful antennas (optical lens systems) allows for both high-speed and long-distance communication. Therefore, higher frequencies do not necessarily lead to shorter communication distances.

3.4 Beamforming and Phased Arrays

The use of phased arrays for electronic beamforming is crucial for this purpose. By providing antennas with signals having phase differences, phased arrays can concentrate beams while manipulating their direction. The performance of a transceiver using an $n \times n$ phased array is depicted in Fig. 15. For a 2×2 phased array, the communication distance is limited to 50 cm. However, with a 128×128 phased array, theoretically, the communication distance can extend up

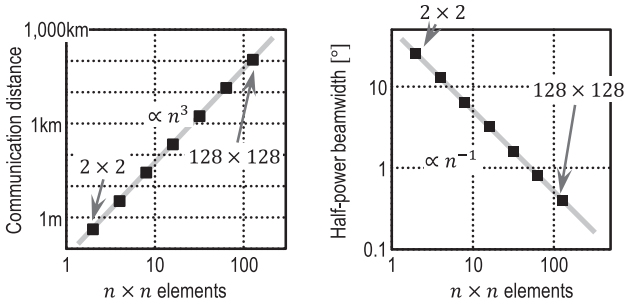

Fig. 15 Relationship between the number of elements n per side of a phased array and the communication distance and half-power beamwidth. Here, the number of antenna elements is assumed to be 1 : 1 in aspect ratio, and the number of elements in the entire phased array is $n \times n$ [32], [33].

to 100 km. Simultaneously, the beamwidth narrows significantly from 28° in a 2 × 2 array to 0.4° in a 128 × 128 array [32], [33].

In summary, this section has explored the theoretical analysis of wireless communication in the terahertz frequency range. It has highlighted the intricate interplay between communication capacity, bandwidth, and communication distance, emphasizing the importance of transceiver performance metrics and the potential of phased arrays for overcoming challenges associated with higher frequencies. The findings contribute valuable insights into the evolving landscape of terahertz wireless communication for Beyond 5G networks.

4. Two-Dimensional Beam-Steerable 300 GHz CMOS Receiver [29]

This section presents our approach to achieving two-dimensional beam steering at 300 GHz using a CMOS receiver. The technical challenge in realizing phased arrays at 300 GHz lies in the extremely short wavelength, approximately 1 mm. To avoid sidelobe generation in phased arrays, it is essential to array antennas at half-wavelength intervals. In the 300 GHz band, this requires placing antennas every 500 µm. However, creating transmitter and receiver circuits at a 500 µm scale poses significant challenges. Thus, previous reports on phased arrays were limited to one dimension. We introduce a hybrid approach that combines phased arrays for horizontal beam steering and mechanically controlled lenses for vertical beam steering, addressing the limitations of conventional phased arrays.

4.1 Hybrid Beam-Steering Approach

The wavelength constraints at 300 GHz necessitate creative solutions for beam steering. As shown in Fig. 16, while phased arrays can easily manipulate the beam's phase angle for broad beam steering, narrowing the beam requires a significant number of elements, leading to increased power consumption. On the other hand, optical methods excel at beam focusing but struggle with beam steering. Considering the requirements for base stations that need wide horizontal beam steering, as shown in Fig. 17, a hybrid approach utilizing both phased arrays and optical systems becomes a compelling solution.

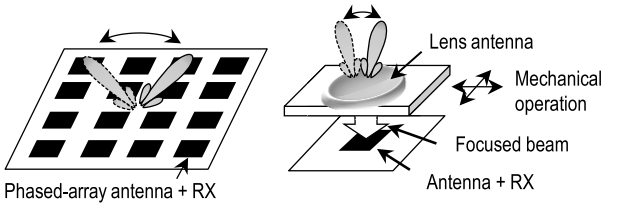

Fig. 16 Two methods for beam manipulation. One is to use a phased array and the other is to mechanically manipulate an optical lens. The latter requires only one antenna and one circuit [29].

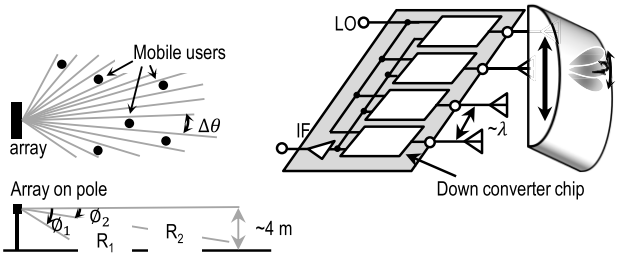

Fig. 17 Overview of operating angles required when the receiver is used as a base station (left). Vertical beam manipulation is required less than horizontal beam manipulation. Therefore, we use a hybrid system with a phased array for horizontal beam manipulation and mechanical manipulation of the optical lens for vertical beam manipulation (right) [29].

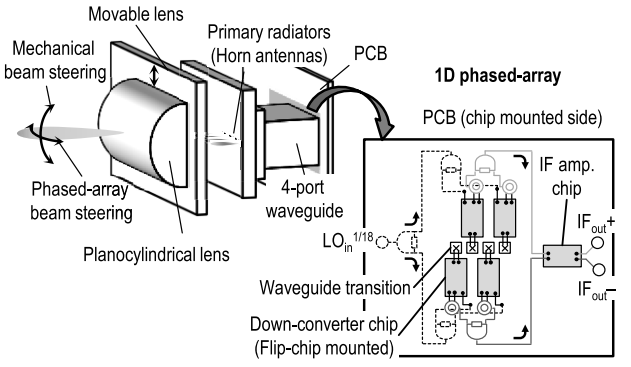

Fig. 18 Overall view of the 2D beam manipulation receiver using the hybrid method. Four CMOS receivers with built-in phase shifters are used for the phased array, which are placed opposite each other. They are power-combined on board and input to an intermediate frequency (IF) amplifier [29].

The proposed hybrid approach, illustrated in Fig. 18, leverages phased arrays for horizontal beam steering and mechanically controlled planocylindrical lenses for vertical beam steering. To address the challenge of narrow antenna pitch, an opposing arrangement of CMOS chips connected to adjacent antennas is employed, allowing the reduction of antenna pitch to half the CMOS pitch. A phase shifter is incorporated in the local oscillator (LO) signal generator supplied to the down-conversion mixer of the CMOS receiver to enable phased array operation by changing the phase.

4.2 Receiver Module

Figure 19 showcases the PCB implementation of the two-dimensional beam-steerable 300 GHz CMOS receiver, featuring a frequency converter with four embedded phase shifters connected to the antennas. The output is power combined on the PCB and fed into the intermediate frequency (IF) amplifier. The backside of the flip-chip mounted CMOS integrated circuits has an array of miniaturized waveguide antennas. Figure 20 provides an overview of the entire two-dimensional beam-steerable 300 GHz CMOS receiver. The focused beam is manipulated by electronic beam steering using a horizontal phased array and mechanical beam steering using a vertical plannocylindrical lens.

4.3 2D Beam Steering Measurement Results and Possibilities Beyond

Figure 21 displays the antenna gains in the vertical (H-plane) and horizontal (E-plane) directions. In this experiment, a phased array with only four elements is used in the horizontal (E-plane) direction. Therefore, a relatively wide range of signals can be received in the horizontal direction, but the number of elements must be increased to achieve higher antenna gain. The vertical (H-plane) planar cylindrical antenna shows beam focusing that reaches antenna gains up to 32 dBi. Vertical beam steering capabilities extend to ±10 degrees, while horizontal beam steering achieves ±14 degrees. Note that this receiver can receive signals up to 52 Gb/s by using 16QAM. This configuration enables versatile beam steering for diverse communication scenarios.

It is important to point out the new possibilities offered by ultrahigh-speed wireless communications. For broadband communications, designs that operate with minimal receive power (sub-nanowatts) relative to transmit power are usually preferred. If ultrahigh-speed wireless communications can be achieved using a sub-terahertz receiver such as the one proposed here, it must operate at the microwatt level of receiving power. This will improve the power propagation efficiency between the transmitter and receiver, thus enabling power-efficient wireless communication. If the beams are extremely narrow, it is also possible to use multiple beams simultaneously in the same space. This implies that numerous simultaneous connectivity can be achieved.

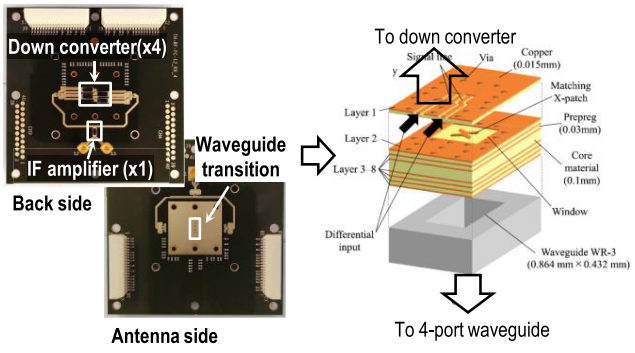

Fig. 19 Photograph of a PCB of a 300-GHz CMOS receiver capable of two-dimensional beam manipulation (left) and a differential transmission line and waveguide converter mounted on the PCB (right); differential signals are used to connect the PCB to the CMOS chip [29].

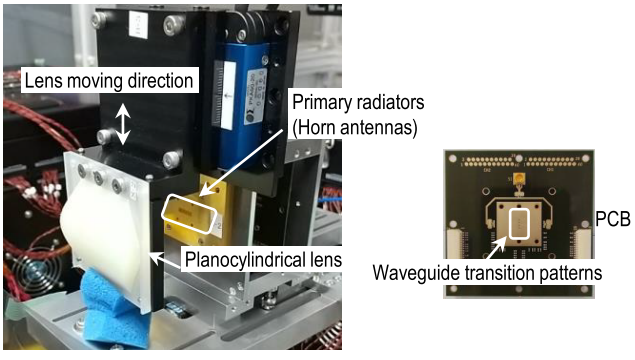

Fig. 20 Overall view of a 300-GHz CMOS receiver capable of two-dimensional beam steering. The vertical beam is steered by moving a planocylindrical lens up and down. The horizontal beam is steered by phased array [29].

5. Conclusion

The pursuit of wireless communication in the 300 GHz band, specifically targeting the continuous 44 GHz bandwidth from 252 GHz to 296 GHz, holds significant promise as a cornerstone for 6G communication. While terahertz communication has traditionally garnered attention for its wide bandwidth, our focus on the 300 GHz band reveals the potential for not only high-speed communication but also the concurrent realization of high energy efficiency and numerous simultaneous connectivity.

We have introduced performance metrics, EIRP_{λ} and EINF_{λ}, as key indicators for transmitter and receiver performance. Demonstrating that these performance metrics remain consistent, and assuming conventional bandwidth and communication capacity, we have shown that communication distance is independent of carrier frequency.

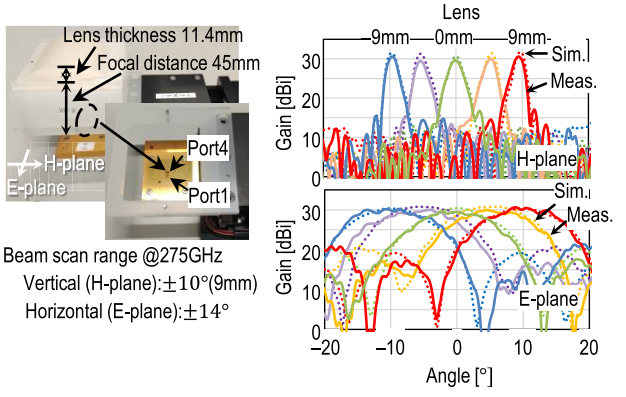

Fig. 21 Photograph of the inside of a 300-GHz CMOS receiver capable of 2-D beam steering (left) and simulation and measurement results of 2-D beam steering (right) [29].

Terahertz waves, residing in the electromagnetic spectrum between radio waves and optics, present a unique opportunity. Radio waves have facilitated wireless communication, providing convenience to people, while optics, through optical fiber communication, has enabled high-capacity data transmission and efficient communication. Terahertz communication, embodying characteristics between radio waves and optics, not only holds the promise of high-speed communication but also offers the potential for a new era of wireless communication characterized by convenience and efficiency. The key to realizing these advancements lies in the enhancement of antenna gain, facilitating beam focusing, and precise beam steering.

As these technologies continue to advance, we anticipate the unfolding of a new paradigm in wireless communication. The combined forces of enhanced antenna gain, beam concentration, and beam steering not only pave the way for unprecedented high-speed communication but also lay the foundation for a wireless communication landscape characterized by unparalleled convenience and efficiency. We look forward to the realization of these technological breakthroughs, anticipating a future where terahertz communication reshapes the landscape of wireless communication.

Acknowledgments

This research was partially supported by the Ministry of Internal Affairs and Communications (JPJ000254) and the Japan Society for the Promotion of Science (JSPS) Grant-in-Aid for Scientific Research No. 22H00217. This work includes joint research results with NICT, Panasonic, THine Electronics, Nagoya Institute of Technology, Tokyo University of Science, and Tokuyama National College of Technology. We would like to express our deepest gratitude to all those involved in and supporting this project.

References

[1] T. Kürner, I. Kallfass, K. Ajito, A. Kasamatsu, D. Britz, and S. Priebe, "What's next? Wireless communication beyond 60 GHz," Tutorial of IEEE 802.15 IG THz, IEEE 802 Plenary, July 2012. (https://mentor.ieee.org/802.15/dcn/12/15-12-0320-02-0thz-what-s-next-wireless-communication-beyond-60-ghz-tutorial-ig-thz.pdf)

[2] "White paper 5G evolution and 6G," NTT DOCOMO, INC., Jan. 2020. (https://www.nttdocomo.co.jp/english/binary/pdf/corporate/technology/whitepaper_6g/DOCOMO_6G_White_PaperEN_20200124.pdf)

[3] G. Ducournau and T. Nagatsuma, "Wireless communications in the THz range," Fundamentals of Terahertz Devices and Applications, pp.479–510, 2021.

[4] T.K. Nguyen, S. Kim, F. Rotermund, and I. Park, "Design of a wideband continuous-wave photomixer antenna for terahertz wireless communication systems," Journal of Electromagnetic Waves and Applications, vol.28, no.8, pp.976–988, 2014.

[5] G. Ducournau, P. Szriftgiser, A. Beck, D. Bacquet, F. Pavanello, E. Peytavit, M. Zaknoune, T. Akalin, and J.-F. Lampin, "Ultrawide-bandwidth single-channel 0.4-THz wireless link combining broadband quasi-optic photomixer and coherent detection," IEEE Trans. Terahertz Sci. Technol., vol.4, no.3, pp.328–337, 2014.

[6] G Ducournau, P. Szriftgiser, D. Bacquet, A. Beck, T. Akalin, E. Peytavit, M. Zaknoune, and J.F. Lampin, "Optically power supplied Gbit/s wireless hotspot using 1.55 μm THz photomixer and heterodyne detection at 200 GHz," Electron. Lett., vol.46, no.19, pp.1349–1351, 2010.

[7] W.R. Deal, A. Zamora, K. Leong, P. Liu, W. Yoshida, J. Zhou, M. Lange, B. Gorospe, K. Nguyen, and X.B. Mei, "A 670 GHz low noise amplifier with <10 dB packaged noise figure," IEEE Microw. Wirel. Compon. Lett., vol.26, no.10, pp.837–839, 2016 (DOI: 10.1109/LMWC.2016.2605458).

[8] I. Kallfass, F. Boes, T. Messinger, J. Antes, A. Inam, U. Lewark, A. Tessmann, and R. Henneberger, "64 Gbit/s transmission over 850 m fixed wireless link at 240 GHz carrier frequency," J. Infrared Millim. Terahertz Waves, vol.36, pp.221–233, 2015 (DOI: 10.1007/s10762-014-0140-6).

[9] A. Fox, B. Heinemann, H. Rücker, R. Barth, G.G. Fischer, C. Wipf, S. Marschmeyer, K. Aufinger, J. Böck, S. Boguth, H. Knapp, R. Lachner, W. Liebl, D. Manger, T.F. Meister, A. Pribil, and J. Wursthorn, "Advanced heterojunction bipolar transistor for half-THz SiGe BiCMOS technology," IEEE Electron Device Lett., vol.36, no.7, pp.642–644, 2015 (DOI: 10.1109/LED.2015.2432130).

[10] N. Sarmah, J. Grzyb, K. Statnikov, S. Malz, P.R. Vazquez, W. Föerster, B. Heinemann, and U.R. Pfeiffer, "A fully integrated 240 GHz directconversion quadrature transmitter and receiver chipset in SiGe technology," IEEE Trans. Microw. Theory Tech., vol.64, no.2, pp.562–574, 2016 (DOI: 10.1109/TMTT.2015.2504930).

[11] I. Kallfass, I. Dan, S. Rey, P. Harati, J. Antes, A. Tessmann, S. Wagner, M. Kuri, R. Weber, H. Massler, A. Leuther, T. Merkle, and T. Kürner, "Towards MMIC-based 300 GHz indoor wireless communication systems," IEICE Trans. Electron., vol.E98-C, no.12, pp.1081–1090, Dec. 2015 (DOI: 10.1587/transele.E98.C.1081).

[12] S. Kim, J. Yun, D. Yoon, M. Kim, J.-S. Rieh, M. Urteaga, and S. Jeon, "300 GHz integrated heterodyne receiver and transmitter with on-chip fundamental local oscillator and mixers," IEEE Trans. Terahertz Sci. Technol., vol.5, no.1, pp.92–101, 2015 (DOI: 10.1109/TTHZ.2014.2364454).

[13] S. Hu, Y.-Z. Xiong, B. Zhang, L. Wang, T.-G. Lim, M. Je, and M. Madihian, "A SiGe BiCMOS transmitter/receiver chipset with on-chip SIW antennas for terahertz applications," IEEE J. Solid-State Circuits, vol.47, no.11, pp.2654–2664, 2012 (DOI: 10.1109/JSSC.2012.2211658).

[14] S. Kang, S.V. Thyagarajan, and A.M. Niknejad, "A 240 GHz fully integrated wideband QPSK transmitter in 65 nm CMOS," IEEE J. Solid-State Circuits, vol.50, no.10, pp.2256–2267, 2015 (DOI: 10.1109/JSSC.2015.2467179).

[15] J.-D. Park, S. Kang, S.V. Thyagarajan, E. Alon, and A.M. Niknejad, "A 260 GHz fully integrated CMOS transceiver for wireless chip-to-chip communication," Symp. VLSI Circuits, pp.48–49, 2012 (DOI: 10.1109/VLSIC.2012.6243783).

[16] D. Lopez-Diaz, I. Kallfass, A. Tessmann, A. Leuther, S. Wagner, M. Schlechtweg, and O. Ambacher, "A subharmonic chipset for gigabit communication around 240 GHz," IEEE MTT-S Int. Microw. Symp., 2012 (DOI: 10.1109/MWSYM.2012.6258404).

[17] I. Abdo, T. Fujimura, T. Miura, K.K. Tokgoz, H. Hamada, H. Nosaka, A. Shirane, and K. Okada, "A 300 GHz wireless transceiver in 65 nm CMOS for IEEE802.15.3d using push-push subharmonic mixer," IEEE/MTT-S Int. Microwave Symp., pp.623–626, 2020 (DOI: 10.1109/IMS30576.2020.9224033).

[18] K. Katayama, K. Takano, S. Amakawa, S. Hara, A. Kasamatsu, K. Mizuno, K. Takahashi, T. Yoshida, and M. Fujishima, "A 300 GHz CMOS transmitter with 32-QAM 17.5 Gb/s/ch capability over six channels," IEEE J. Solid-State Circuits, vol.51, no.12, pp.3037–3048, 2016 (DOI: 10.1109/JSSC.2016.2602223).

[19] K. Katayama, K. Takano, S. Amakawa, S. Hara, A. Kasamatsu, K. Mizuno, K. Takahashi, T. Yoshida, and M. Fujishima, "A 300GHz 40nm CMOS transmitter with 32-QAM 17.5 Gb/s/ch capability over 6 channels," ISSCC Dig. Tech. Papers, pp.342–343, 2016 (DOI: 10.1109/ISSCC.2016.7418047).

[20] K. Katayama, K. Takano, S. Amakawa, S. Hara, A. Kasamatsu, K. Mizuno, K. Takahashi, T. Yoshida, and M. Fujishima, "A 300 GHz CMOS Transmitter with 32-QAM 17.5 Gb/s/ch Capability Over Six Channels," IEEE J. Solid-State Circuits, vol.51, no.12, pp.3037–3048, 2016 (DOI: 10.1109/JSSC.2016.2602223).
[21] M. Fujishima, "Future of 300-GHz-band wireless communications and their enabler, CMOS transceiver technologies," Ext. Abstr. Solid State Devices and Materials, 207, 2020.
[22] K. Takano, S. Amakawa, K. Katayama, S. Hara, R. Dong, A. Kasamatsu, I. Hosako, K. Mizuno, K. Takahashi, T. Yoshida, and M. Fujishima, "A 105 Gb/s 300 GHz CMOS transmitter," ISSCC Dig. Tech. Papers, pp.308–309, 2017 (DOI: 10.1109/ISSCC.2017.7870384).
[23] S. Hara, K. Katayama, K. Takano, R. Dong, I. Watanabe, N. Sekine, A. Kasamatsu, T. Yoshida, S. Amakawa, and M. Fujishima, "A 32 Gbit/s 16 QAM CMOS receiver in 300 GHz band," IEEE Int. Microwave Symp., pp.1703–1706, 2017 (DOI: 10.1109/MWSYM.2017.8058969).
[24] S. Hara, K. Katayama, K. Takano, R. Dong, I. Watanabe, N. Sekine, A. Kasamatsu, T. Yoshida, S. Amakawa, and M. Fujishima, "32-Gbit/s CMOS receivers in 300-GHz band," IEICE Trans. Electron., vol.E101-C, no.7, pp.464–471, 2018 (DOI: 10.1587/transele.E101.C.464).
[25] S. Lee, R. Dong, T. Yoshida, S. Amakawa, S. Hara, A. Kasamatsu, J. Sato, and M. Fujishima, "An 80Gb/s 300GHz-band single-chip CMOS transceiver," ISSCC Dig. Tech. Papers, pp.170–172, 2019 (DOI: 10.1109/ISSCC.2019.8662314).
[26] S. Lee, S. Hara, T. Yoshida, S. Amakawa, R. Dong, A. Kasamatsu, J. Sato, and M. Fujishima, "An 80-Gb/s 300-GHz-band single-chip CMOS transceiver," IEEE J. Solid-State Circuits, vol.54, no.12, pp.3577–3588, 2019 (DOI: 10.1109/JSSC.2019.2944855).
[27] S. Hara, R. Dong, S. Lee, K. Takano, N. Toshida, S. Tanoi, T. Hagino, M.H. Mubarak, N. Sekine, I. Watanabe, A. Kasamatsu, K. Sakakibara, S. Kubo, S. Miura, Y. Umeda, T. Yoshida, S. Amakawa, and M. Fujishima, "A 76-Gbit/s 265-GHz CMOS receiver," 2021 IEEE Asian Solid-State Circuits Conference (A-SSCC), pp.1–3. IEEE, 2021.
[28] S. Hara, R. Dong, S. Lee, K. Takano, N. Toshida, A. Kasamatsu, K. Sakakibara, T. Yoshida, S. Amakawa, and M. Fujishima, "A 76-Gbit/s 265-GHz CMOS receiver with WR-3.4 waveguide interface," IEEE J. Solid-State Circuits, vol.57, no.10, pp.2988–2998, 2022.
[29] T. Yoshida, S. Hara, T. Hagino, M. Mubarak, A. Kasamatsu, K. Takano, Y. Sugimoto, K. Sakakibara, S. Amakawa, and M. Fujishima, "A 2D beam-steerable 252–285-GHz 25.8-Gbit/s CMOS receiver module," 2023 IEEE Asian Solid-State Circuits Conference (A-SSCC), pp.1–3, IEEE, 2023.
[30] "Sharing and compatibility studies between land-mobile, fixed and passive services in the frequency range 275–450 GHz," Report ITU-R SM.2450-0, June 2019 (https://www.itu.int/pub/R-REP-SM.2450-2019).
[31] IEEE Standard for High Data Rate Wireless Multi-Media Networks, Amendment 2: 100 Gb/s Wireless Switched Point-to-Point Physical Layer, IEEE Computer Society sponsored by the LAN/MAN Standards Committee https://standards.ieee.org/standard/802_15_3d-2017.html (2017).
[32] M. Fujishima, "Future of 300 GHz band wireless communications and their enabler, CMOS transceiver technologies," Jpn. J. Appl. Phys., vol.60, SB0803, 2021 (DOI: 10.35848/1347-4065/abdf24).
[33] M. Fujishima, "Overview of sub-terahertz communication and 300GHz CMOS transceivers," IEICE Electron. Express, vol.18, no.8, 20212002, 2021.
[34] H.T. Friis, "A note on a simple transmission formula," Proc. IRE, vol.34, no.5, pp.254–256, 1946 (DOI: 10.1109/JRPROC.1946.234568).
[35] L. Press, "Inter-satellite laser link update," CircleID, 2019, https://circleid.com/posts/20190906_inter_satellite_laser_link_update

Minoru Fujishima received his Ph.D. from the University of Tokyo in 1993, and after working as an assistant and associate professor at the University of Tokyo, he has been a full professor at Hiroshima University since 2009. He was a visiting professor at the Katholieke Universiteit Leuven, Belgium, from 1998 to 2000. He was formerly engaged in research on design and modeling of CMOS and BiCMOS circuits, nonlinear circuits, single-electron circuits, and quantum computing circuits, and is currently interested in research on ultrahigh-speed wireless communications using terahertz. He served as a distinguished lecturer of the IEEE Solid State Circuits Society, Chair of the IEEE Japan Council Chapter Operations Committee, and President of the Electronics Society of the IEICE. He is a fellow of the IEICE, a senior member of the IEEE, and a member of the Japan Society of Applied Physics.